NUCLEAR INSTRUMENTS AND METHODS 154 (1978) 501-508 ; © NORTH-HOLLAND PUBLISHING CO.

MONTE CARLO CALCULATION OF EFFICIENCIES OF RIGHT-CIRCULAR CYLINDRICAL NaI DETECTORS FOR ARBITRARILY LOCATED POINT SOURCES

G. B. BEAM, L. WIELOPOLSKI, R. P. GARDNER and K. VERGHESE

Department of Nuclear Engineering, North Carolina State University, Raleigh, North Carolina 27650, U.S.A.

Received 3 March 1978

An efficient Monte Carlo program for calculation of total intrinsic efficiency, peak-to-total ratio and source intrinsic efficiency of bare right-circular cylindrical NaI(Tl) detectors from an arbitrarily located isotropic point source emitting photons of energy 1 MeV or below is outlined. Total variance reduction based on physical principles is used throughout to insure that each photon history is successful in order to minimize computer time. Results show close agreement with other Monte Carlo calculations for sources located along the detector axis and with experiments for sources located off-axis.

1. Introduction

Detector efficiencies as a function of energy for scintillation detectors can be obtained either experimentally or by Monte Carlo simulation. The experimental method is limited primarily to gamma-ray energies of the common radioisotope sources. In order to obtain efficiencies for intermediate energies interpolation is required. On the other hand Monte Carlo calculations can provide NaI detector efficiencies at any specified energy. Such calculations have been reported by Miller and Snow[1]), Zerby and Moran[2]), and Seltzer and Berger[3]) for point isotropic sources located on the axis of right-circular cylindrical detectors. Marshall has written a program for calculating the response of scintillators in complex detector geometries but few details are given[4]).

This paper describes a Monte Carlo calculation which determines the intrinsic and photopeak detector efficiency of a right-circular cylindrical NaI detector for a monoenergetic gamma-ray source located at any arbitrary position. The Monte Carlo treatment used here differs from most other such calculations in that total variance reduction is incorporated. The program does not take into account the cladding material encasing the scintillation crystal or the photomultiplier mounting. The analysis considers only Compton and photoelectric interactions; i.e., photons with energy of 1 MeV or less. Because the production of secondary electrons is neglected, all energy is assumed to be deposited at the interaction site.

A description of the Monte Carlo analysis and a flow chart of the program logic are presented. Results obtained in this work are compared with published Monte Carlo data for bare detectors exposed to point sources located on the detector axis and with experimental results for point sources located off the axis of the detector.

2. Solid angle and photon detection

The Monte Carlo treatment consists of following and categorizing a large number of photon histories from emission at the source to absorption within the detector. Random number and probability theory, combined with known transport distributions are used to locate the photon collison site, as well as trajectory, energy and direction throughout each history. Three variance reduction steps are employed during each history:

a) Each gamma-ray is forced to strike the detector;
b) each gamma-ray is forced to interact within the bounds of the detector; i.e., photons are not allowed to escape from the detector and
c) each interaction is forced to be a Compton scattering event. Each photon history is terminated when either the weight of a scattering interaction (i.e., the ratio of scattering to total cross section) or the energy of the photon falls below a specified minimum (e.g., 10^{-10} or 0.01 MeV).

Any possibility of bias due to these variance reduction techniques is eliminated by calculating appropriate weights for each of the above forced events using well-defined physical and geometrical principles. For each history there are three decisions to be made:

a) Does the gamma-ray strike the detector on the top or side?

b) How far does the photon travel before it interacts within the detector?
c) What new energy and direction does the photon have after undergoing a Compton interaction?

Decisions (b) and (c) are repeated until either the photon weight or energy drops below the appropriate threshold value.

2.1. Determination of solid angle and detector entrance point

For each photon emitted from a point source, the probability of striking the detector and the point where the photon actually enters the detector must be known. The former is accomplished by a Monte Carlo calculation of the solid angle subtended by a cylindrical detector at an arbitrary point[5]). From input the position of the point relative to the detector is known. The two cases to be studied are:

1) a point source located in such a position that photons can enter either through the top or side of the detector (fig. 1), and
2) a point source located within the cylindrical region directly above the circular face of the detector (fig.2).

Considering fig. 1 first, define the angle α_{max} by

$$\alpha_{max} = \arcsin(r/\rho), \tag{1}$$

where r is the radius of the detector and ρ is the distance from the center of the detector to a line parallel to the detector axis containing the point source. The actual angle, α, is derived from

$$n = \left(\int_{-\alpha_{max}}^{\alpha} d\alpha/2\pi\right) \Big/ \left(\int_{-\alpha_{max}}^{\alpha_{max}} d\alpha/2\pi\right),$$

where n is a random selected from a uniform distribution between 0 and 1. Consequently,

$$\alpha = \alpha_{max}(2n-1), \qquad -\alpha_{max} \leq \alpha \leq \alpha_{max}. \tag{2}$$

The weighting factor associated with this selection of α, $w(\alpha)$, is given by

$$w(\alpha) = \left(\int_{-\alpha_{max}}^{\alpha_{max}} d\alpha/2\pi\right) \Big/ \left(\int_{0}^{2\pi} d\alpha/2\pi\right),$$

$$w(\alpha) = \alpha_{max}/\pi. \tag{3}$$

Once α is selected, the points A, B, C and D in fig. 1 define the plane through which the photon must enter the detector for point sources located at S_1 and S_2. To determine the position along this plane through which the photon enters, the angles θ_{max}, θ_{cri} and θ_{min} must be defined. Referring to fig. 1, the line segments $\overline{OB}$ and $\overline{OA}$ are determined by

$$OB = \rho\cos\alpha - (r^2 - \rho^2\sin^2\alpha)^{1/2} \tag{4}$$

and

$$OA = \rho\cos\alpha + (r^2 - \rho^2\sin^2\alpha)^{1/2}. \tag{5}$$

When the source is located above the top plane of the detector, for example at S_1 (i.e., when $h \geq 0$),

$$\theta_{max} = \arctan(OA/h), \tag{6a}$$

$$\theta_{cri} = \arctan(OB/h), \tag{6b}$$

and

$$\theta_{min} = \arctan(OB/(h+l)) \tag{6c}$$

In the case where $h = 0$ (when the source is located at O),

$$\theta_{max} = \pi/2, \tag{7a}$$

$$\theta_{cri} = \pi/2, \tag{7b}$$

and

$$\theta_{min} = \arctan(OB/l) \tag{7c}$$

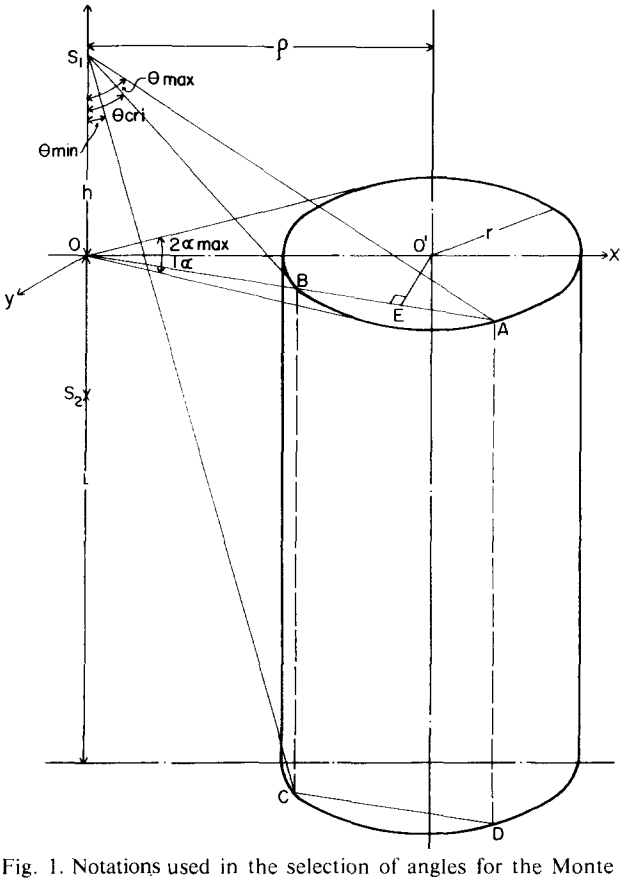

Fig. 1. Notations used in the selection of angles for the Monte Carlo calculation.

and for $h<0$, for example at S_2 in fig. 1,

$$\theta_{max} = \pi/2 + \arctan(|h|/OB), \tag{8a}$$

$$\theta_{cri} = \pi/2 + \arctan(|h|/OB), \tag{8b}$$

and

$$\theta_{min} = \arctan[(OB/(l-|h|)]. \tag{8c}$$

The particular angle θ defining the angle along which this photon enters the detector is chosen using another rectangularly distributed random number n.

$$n = \int_{\theta_{min}}^{\theta} (1/2)\sin\theta\,d\theta \Big/ \int_{\theta_{min}}^{\theta_{max}} (1/2)\sin\theta\,d\theta \tag{9a}$$

and

$$\theta = \arccos\{\cos(\theta_{min}) - n[\cos(\theta_{min}) - \cos(\theta_{max})]\}. \tag{9b}$$

θ is tested to see if the photon enters the top or side of the detector by comparing it to the angle θ_{cri} defined by eq. (6b). The appropriate weighting factor, $w(\theta)$, for this selection of θ is given by

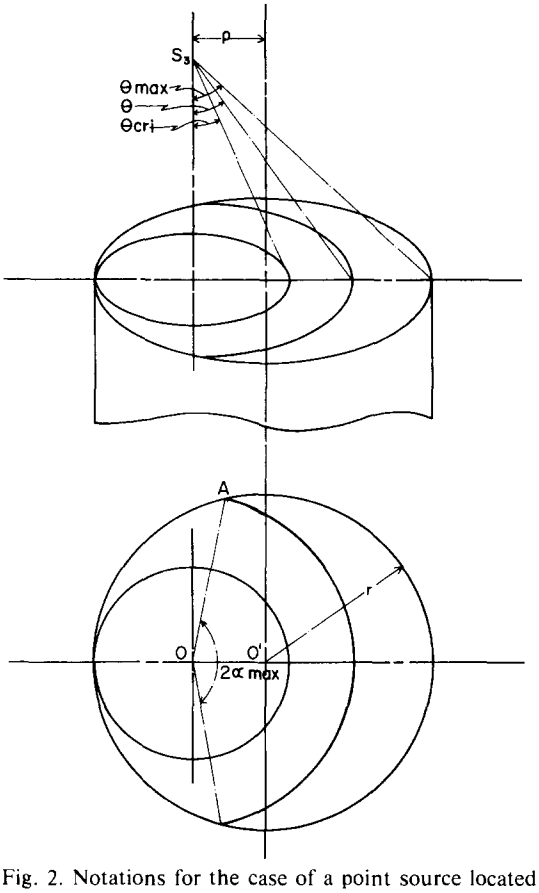

Fig. 2. Notations for the case of a point source located directly above the circular face of the detector.

$$w(\theta) = \int_{\theta_{min}}^{\theta_{max}} (1/2)\sin\theta\,d\theta \Big/ \int_{0}^{\pi} (1/2)\sin\theta\,d\theta,$$

$$w(\theta) = [\cos(\theta_{min}) - \cos(\theta_{max})]/2. \tag{10}$$

To consider the last case when the point is located at S_3 in fig. 2, we notice that θ_{max} remains constant. Therefore, θ is calculated first and α is determined knowing the value of θ. In this case the critical angle, θ_{cri}, defines an angle below which angle α may vary over 2π and above which the variation of α is limited to $2\alpha_{max}$. According to fig. 2, θ_{max} and θ_{cri} are given by

$$\theta_{max} = \arctan[(r+\rho)/h] \tag{11a}$$

$$\theta_{cri} = \arctan[(r-\rho)/h] \tag{11b}$$

and $\theta_{min} = 0$. θ is chosen according to eq. (9b). Once again θ is checked for magnitude lower or higher than θ_{cri}. In the first case, angle α varies over 2π and the associated weighting factor is simply one. For $\theta > \theta_{cri}$, α is restricted to $2\alpha_{max}$ given by

$$\alpha_{max} = \arccos[(\rho^2 + h^2\tan^2\theta - r^2)/2h\rho\tan\theta] \tag{12}$$

and α is chosen from eq. (2). The weighting factor is given according to eq. (3). The total weighting factor for any selection of α and θ in fig. 1 or 2 is given by

$$W_i = w(\theta)\,w(\alpha), \tag{13}$$

where W_i represents the solid angle subtended for this particular selection of α and θ. The estimate of the solid angle, Ω, is given by the mean value

$$\Omega = \left(\frac{1}{N}\right)\sum_{i=1}^{N} W_i, \tag{14}$$

where N is the total number of histories. The standard deviation of Ω is obtained from

$$\sigma_\Omega = \left[\frac{1}{N(N-1)}\left(\sum_{i=1}^{N} W_i^2 - N\Omega\right)\right]^{1/2}. \tag{15}$$

2.2. Determination of initial direction cosines

Knowing the point of entrance into the detector by the angles θ and α, the point of exit from the detector along this path may also be found. Care must be taken in determining if the photon path exits the detector from the bottom or side of the detector. Considering fig. 3, basic trigonometric relationships can be used to find the distance a photon can travel through the detector assuming no interaction. Again, there are two cases to be

considered, each having two subcases. The photon may enter from the top or side and then may exit either through the bottom or side. Fig. 3 shows these four different cases and the appropriate expressions for the maximum distance the photon can travel through the detector.

Knowing entrance and exit points and the effective distance traveled through the detector, the calculation of the initial direction cosines of the photon are given by

$$\cos\alpha = (X_1 - X_0)/d, \tag{16a}$$

$$\cos\beta = (Y_1 - Y_0)/d, \tag{16b}$$

$$\cos\gamma = (Z_1 - Z_0)/d, \tag{16c}$$

where (X_1, Y_1, Z_1) and (X_0, Y_0, Z_0) are the coordinates of the exit point and the entrance point, respectively.

2.3. Determination of attenuation cross-sections

Let σ and τ be the total Compton and photoelectric coefficients, respectively, of the NaI crystal. Then the total attenuation cross section is given by

$$\mu = \sigma + \tau. \tag{17}$$

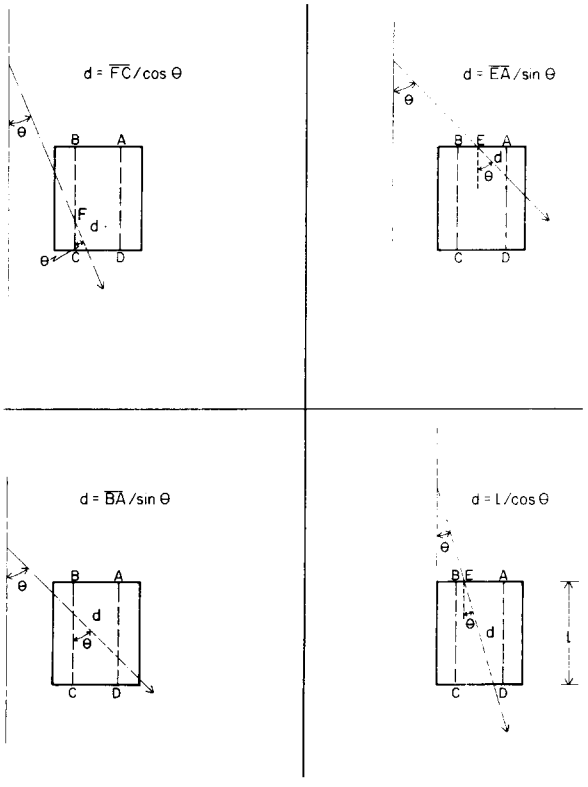

Fig. 3. The four possible cases of travel of photons through the detector.

2.4. Determination of probability of interaction

Source photons entering the detector were initiated with a probability of existence as weight, W, equal to 1.0. This weight was reduced after each interaction by the ratio of the scattering to the total cross section and the probability of interaction within the detector. A photon history was terminated and the photon was considered absorbed only if either the weight dropped below an assigned value (10^{-10}) or if the degraded photon energy dropped below a designated value (e.g., 0.01 MeV). The probability of an interaction within the detector was defined as

$$W = \int_0^d e^{-\mu x}\,dx \Big/ \int_0^\infty e^{-\mu x}\,dx = 1 - e^{-\mu d}, \tag{18}$$

where μ is the total linear attenuation as calculated in section 2.3 and d is the effective distance. Photon path lengths between interaction sites were determined from

$$n = \int_0^l e^{-\mu x}\,dx \Big/ \int_0^d e^{-\mu x}\,dx,$$

$$l = (1/\mu)\ln\{1 - n(1 - e^{-\mu d})\}, \tag{19}$$

where n is a rectangularly distributed random number between 0 and 1.

2.5. Determination of change in direction and energy after scatter

When the photon undergoes a Compton interaction, the reduced energy and new direction of the photon must be found. The interaction sites P_N and P_{N-1} are defined by (X_N, Y_N, Z_N) and $(X_{N-1}, Y_{N-1}, Z_{N-1})$, respectively, where N denotes the Nth interaction site. Thus, the coordinates of the $(N+1)$ interaction site are found by

$$X_{N+1} = l\cos\alpha + X_N, \tag{20a}$$

$$Y_{N+1} = l\cos\beta + Y_N, \tag{20b}$$

$$Z_{N+1} = l\cos\gamma + Z_N, \tag{20c}$$

where cos α, cos β, cos γ are the direction cosines after the Nth interaction.

Energy is reduced in accord with the Klein–Nishina differential scattering cross-section [as discussed by Dunn and Gardner[6]]. The scattering angle θ is given by the Compton scattering

law.

$$\cos\theta = 1+0.511/E_0-0.511/E, \tag{21}$$

where E_0 is the initial photon energy before scattering and E is the photon energy afterwards. The azimuthal angle of the scattered path relative to the incident path is found at random from 0 to 2π by

$$\phi = 2\pi n. \tag{22}$$

The new direction cosines after scattering are

$$\cos\alpha' = \cos\alpha\cos\theta + (\cos\gamma\cos\alpha\sin\theta\cos\phi - \\ - \cos\beta\sin\theta\sin\phi)/(1-\cos^2\gamma)^{\frac{1}{2}}, \tag{23a}$$

$$\cos\beta' = \cos\beta\cos\theta + (\cos\gamma\cos\beta\sin\theta\cos\phi + \\ + \cos\alpha\sin\theta\sin\phi)/(1-\cos^2\gamma)^{\frac{1}{2}}, \tag{23b}$$

$$\cos\gamma' = \cos\gamma\cos\theta - (1-\cos^2\gamma)^{\frac{1}{2}}\sin\theta\cos\phi, \tag{23c}$$

except in the case where $(1-\cos^2\gamma)$ approaches zero, in which case the degenerate form

$$\cos\alpha' = \sin\theta\cos\phi, \tag{24a}$$

$$\cos\beta' = \sin\theta\sin\phi, \tag{24b}$$

$$\cos\gamma' = \cos\gamma\cos\phi, \tag{24c}$$

is used. With a new direction the new distance a photon can travel from the interaction site to the wall of the detector along the scattering path is required. First, consider the case where the photon tries to exit through the side of the detector. This distance can be given by simultaneously solving the equation for a circle on the right circular cylindrical detector and the equation for the straight line path of the photon.

$$R^2 = X_R^2+Y_R^2, \tag{25a}$$

$$d = (X_R-X)/\cos\alpha = (Y_R-Y)/\cos\beta \\ = (Z_R-Z)/\cos\gamma,$$

where (X_R, Y_R, Z_R) are the coordinates of the photon exit point at the surface of the detector and (X, Y, Z) are the coordinates of the present interaction site; d and R are the effective distance and radius of the detector, respectively, therefore:

$$X_R = d\cos\alpha+X, \tag{25b}$$

$$Y_R = d\cos\beta+Y,$$

or substituting into eq. (25a) for X_R and Y_R yields:

$$d^2(\cos^2\alpha+\cos^2\beta) + 2d\,(X\cos\alpha+Y\cos\beta) + \\ + (X^2+Y^2-R^2) = 0, \tag{25c}$$

which can be solved for d. If the photon exits from the side of the detector, then one root is positive and the other is negative. A check for this is done by calculating Z_R and comparing it with the actual Z dimensions of the detector. Thus, $Z_R = d\cos\gamma+Z$. If Z_R is not within the vertical boundaries of the detector, namely $0<Z<l$ (detector length), then the photon is headed toward the top or bottom of the detector and the effective distance is given by

$$d = -(l-Z)/\cos\gamma, \tag{26a}$$

or

$$d = -Z/\cos\gamma, \tag{26b}$$

depending on whether the new direction is positive (upward) or negative (downward).

3. Efficiency calculation

The total intrinsic efficiency is determined by finding the mean average of the weights for the first interaction within the sensitive volume of the detector. Therefore,

$$\varepsilon_{E_0} = (1/N)\sum_{i=1}^{N} W_{i1}\,W_i/\Omega, \tag{27}$$

where N is the total number of histories and W_{i1} is the weight of the first interaction for each history given by eq. (18). The appropriate standard deviation of ε_{E_0} is obtained from the general estimator

$$\sigma_\varepsilon = \left\{[1/N(N-1)]\left(\sum_{i=1}^{N} W_i^2\,W_{i1}^2/\Omega^2 - N\varepsilon_{E_0}^2\right)\right\}^{\frac{1}{2}}. \tag{28}$$

The photopeak efficiency is calculated in the same manner as the intrinsic efficiency except all interactions until the photon is absorbed or killed off are taken into account. Thus,

$$P_\varepsilon = (1/N)\sum_{i=1}^{N}\left\{W_{i1}(\tau_{i1}/\mu_{i1}) + W_{iv}(\tau_{iv}/\mu_{iv})\times \right. \\ \left. \times\left[\prod_{j=2}^{v} W_{i(j-1)}\,\sigma_{i(j-1)}/\mu_{i(j-1)}\right]\right\}, \tag{29}$$

where v is the total number of interactions for the ith particular history. W_i and τ_i are the weights and the photoelectric cross section for the last interaction in the ith history. The standard deviation of P_ε is given by an equation of similar form as the general estimation in eq. (28). The peak-to-total-ratio is given by

$$\text{peak-to-total-ratio} = \frac{P_\varepsilon}{\varepsilon_{E_0}} \tag{30}$$

and its standard deviation is found from

$$\sigma_{\text{peak to total}} = (P_\varepsilon/\varepsilon_{E_0})\,[(\sigma^2_{P_\varepsilon}/P^2_\varepsilon) + (\sigma^2_\varepsilon/\varepsilon_{E_0})]^{\frac{1}{2}}. \quad (31)$$

The total source intrinsic efficiency which includes geometry factor is thus

$$\varepsilon_G = \Omega\varepsilon_{E_0}, \quad (32)$$

where Ω is given by eq. (14). A flow chart of the Monte Carlo program is given in fig. 4.

4. Results

Efficiencies were calculated for two NaI(Tl) detectors at various gamma-ray energies using the Monte Carlo program. All of the photoelectric cross-sections were taken from the tabulation by Storm and Israel[8]). Since tabulated NaI efficiencies are for points located along the axis of the detector, experimental results were used to check the Monte Carlo model for point sources not on the axis.

Figs. 5 and 6 show comparison of our Monte Carlo results with other Monte Carlo calculations

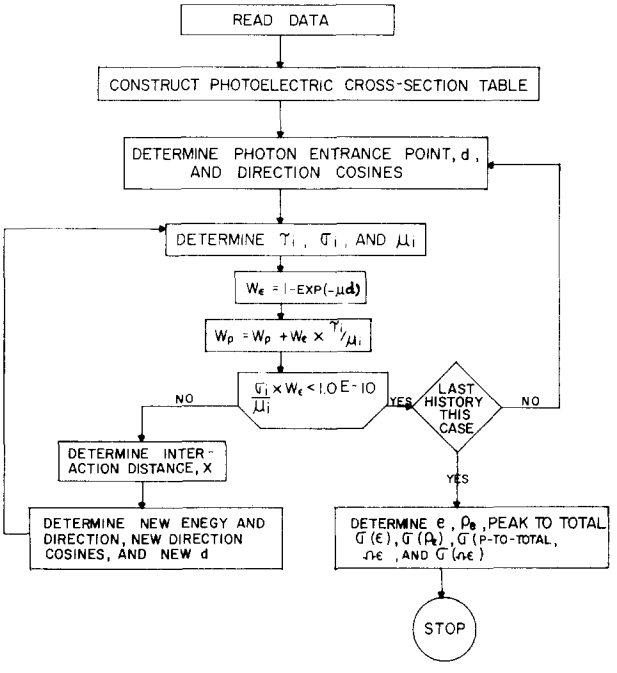

Fig. 4. Flow chart of the Monte Carlo program.

TABLE 1

Point source efficiency values of a 2″×2″ NaI(Tl) crystal for a ^{137}Cs point source.

Angle	ρ (cm) h (cm)	Relative source intrinsic efficiency		Relative source photopeak efficiency (includes geometry effect)	
		experim.	Monte Carlo	experim.	Monte Carlo
0	0 45.0	1.000 ± 0.002	1.000 ± 0.010	1.000 ± 0.002	1.000 ± 0.033
30	22.5 39.0	1.136 ± 0.007	1.057 ± 0.021	1.061 ± 0.006	1.077 ± 0.049
45	31.8 31.8	1.201 ± 0.006	1.123 ± 0.021	1.109 ± 0.007	1.102 ± 0.049
60	39.0 22.5	1.276 ± 0.007	1.172 ± 0.020	1.158 ± 0.006	1.118 ± 0.047
90	45.0 0	1.320 ± 0.008	1.220 ± 0.013	1.197 ± 0.006	1.201 ± 0.043
0	0 15.0	1.000 ± 0.001	1.000 ± 0.020	1.000 ± 0.001	1.000 ± 0.041
30	7.5 13.0	1.051 ± 0.002	1.034 ± 0.023	1.046 ± 0.003	1.042 ± 0.050
45	10.6 10.6	1.151 ± 0.002	1.099 ± 0.023	1.130 ± 0.003	1.071 ± 0.051
60	13.0 7.5	1.244 ± 0.003	1.215 ± 0.024	1.213 ± 0.003	1.177 ± 0.053
90	15.0 0	1.557 ± 0.003	1.414 ± 0.023	1.483 ± 0.003	1.364 ± 0.054

for point sources located on the axis. Excellent agreement is observed between the literature and our model for efficiencies including geometry factor, intrinsic efficiency, and peak-to-total ratios. The relative standard error involved in each calculation was between 1% to 4%.

For sources located away from the detector axis, neither computed nor experimental values were available in the literature for comparison. Therefore, experimental data was collected using a 2″×2″ detector and a small ^{137}Cs source placed at different locations away from the detector axis. Table 1 gives the results of the experiments compared to the calculated values from the Monte Carlo program. Both sets of data are normalized to unity when the source is located on the detector axis. The angle given in table 1 is between the detector axis and the line joining the source point to the center of the top face of the detector. The calculated and experimental efficiencies show reasonable agreement. The experimental values are significantly higher than calculated values in the case of source intrinsic efficiencies. This is presumably due to scattering of photons from the photomultiplier, and from surrounding materials interacting in the crystal. Such effects are not considered in the Monte Carlo model.

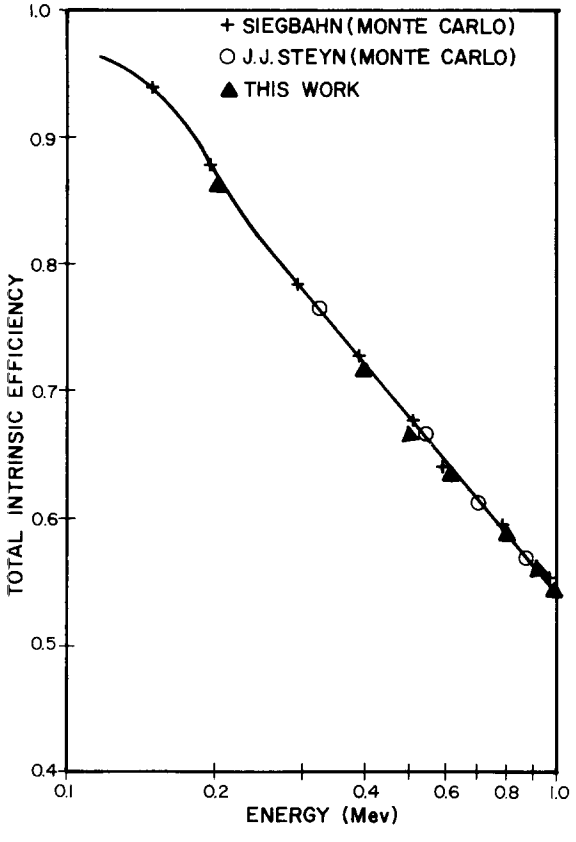

Fig. 5. Total intrinsic efficiency of a 3″×3″ NaI(Tl) detector for a point source located on the axis at 10″ from the circular end.

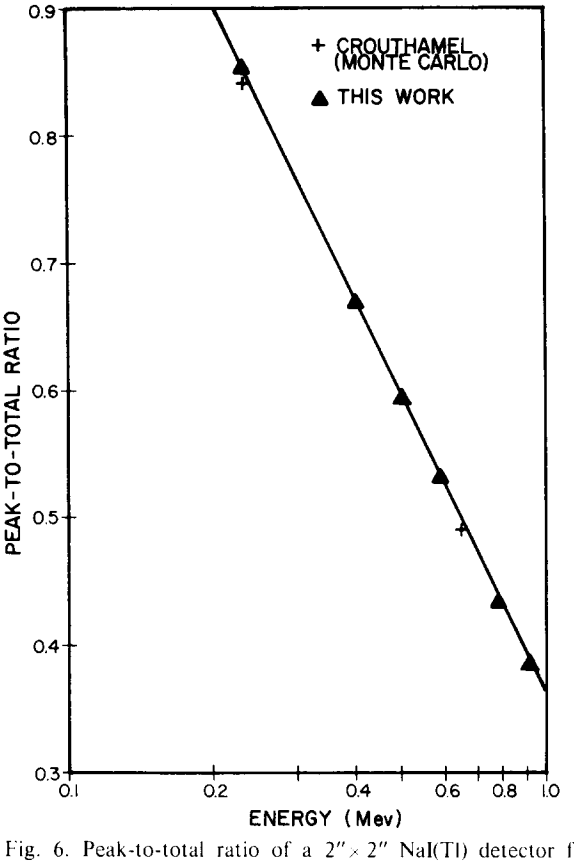

Fig. 6. Peak-to-total ratio of a 2″× 2″ NaI(Tl) detector for a point source located on the axis at 15″ from the circular end.

5. Discussion

Generally speaking, the various variance reduction schemes do not appear to introduce any significant bias. Another form of "killing off the photon" by comparing the ratio of the photoelectric to total cross section against a random number was tried. Computer execution time was shorter because fewer interactions were required to kill off the photon. While the results for the intrinsic efficiency were approximately the same, the photopeak efficiency and its standard deviation deviated from the other method by 4% to 5% for the same number of histories. Both the photopeak efficiency and its standard deviation are based on the number of interactions required to kill off the photon.

The advantage to this new method is that it requires fewer interactions by each photon history, the computer execution time is shorter and, thus, less expensive.

The program was written in FORTRAN IV computer language for use with an IBM 370/165 computer. Typically, the total computer run time to determine the efficiency at five energies from 1MeV to 0.2 MeV on the basis of 1000 histories for a specific size NaI(Tl) detector is approximately 1 min. The program is available from the authors.

In general the Monte Carlo program is expected to give accurate results for incident gamma-ray energies below 1 MeV. The extension of this model to include pair production and cladding effects would greatly benefit the testing of NaI(Tl) detectors of various sizes in different geometries. In addition, the model could be revised to compute the efficiency of a NaI(Tl) detector in a finite uniformly distributed medium.

References

1) W. F. Miller and W. J. Snow, ANL-6318, Argonne National Laboratory (1961).
2) C. D. Zerby and H. S. Moran, Nucl. Instr. and Meth. **14** (1962) 115.
3) J. M. Seltzer and M. J. Berger, ANS Trans. **14** (1971) 124.
4) J. D. Marshall, ANS Trans. **13** (1970) 873.
5) L. Wielopolski, Nucl. Instr. and Meth. **143** (1977) 577.
6) W. L. Dunn and R. P. Gardner, Nucl. Instr. and Meth. **103** (1972) 373.
7) N. M. Schaeffer (Ed.), *Reactor shielding for nuclear engineers*, U.S. Atomic Energy Commission (1973).
8) E. Storm and H. I. Israel, LA-3753, Los Alamos Sci. of Lab. of Univ. of California (1974).